Spin-glass behavior in a three-dimensional antiferromagnet ordered phase: Magnetic structure of $Co_2(OH)(PO_4)$

J. M. Rojo,[1] J. L. Mesa,[1] L. Lezama,[1] J. L. Pizarro,[2] M. I. Arriortua,[2] J. Rodriguez Fernandez,[3] G. E. Barberis,[4] and T. Rojo[1,*]

[1]*Departamento de Química Inorgánica, Facultad de Ciencias, Universidad del País Vasco, E-48080, Bilbao, Spain*

[2]*Departamento de Mineralogía-Petrología, Facultad de Ciencias, Universidad del País Vasco, E-48080, Bilbao, Spain*

[3]*CITIMAC, Facultad de Ciencias, Universidad de Cantabria. Avenida de los Castros, 39005 Santander, Spain*

[4]*Instituto de Física Gleb Wataghin, UNICAMP, 13087-970, Campinas, Sáo Paulo, Brazil*

(Received 21 February 2002; revised manuscript received 16 May 2002; published 6 September 2002)

$Co_2(OH)(PO_4)$ has been prepared from hydrothermal synthesis and characterized from powder x-ray diffraction. The nuclear and magnetic structures have been determined by neutron (D2B and D1B) diffraction data. The structure consists of a three-dimensional framework in which $Co(1)O_5$-trigonal bipyramid dimers and $Co(2)O_6$-octahedra chains are simultaneously present. The EPR spectrum of $Zn_2(OH)(PO_4)$:0.1%Co at 4.2 K shows a strong anisotropy of the *g* factor. The values obtained for the *g* tensor and the hyperfine coupling constants for the octahedral symmetry were $g_1=5.890$, $g_2=4.550$, and $g_3=2.021$ and $A_1=240\times10^{-4}$ cm^{-1}, $A_2=155\times10^{-4}$ cm^{-1}, and $A_3=85\times10^{-4}$ cm^{-1}. Signals corresponding to the five-coordinated Co(II) ions were also observed. Magnetization measurements show the presence of two maxima at circa 75 and 15 K, respectively. The first peak was attributed to a three-dimensional antiferromagnetic ordering and the second one reveals the existence of a spin-glass-like state. This state with a cooperative freezing was also confirmed by both ac susceptibility measurements and magnetic irreversibility observed in the zero-field-cooled–field-cooled signals. From low-temperature neutron-diffraction data, antiferromagnetic ordering is established with an ordering temperature of 71 K. The propagation vector of the magnetic structure is $k=[0,0,0]$. The magnetic moments at 1.7 K are ferromagnetically coupled between CoO_6-octahedra chains and the Co_2O_{10} dimers in the *z* direction. The values obtained for the magnetic moments are: $3.39(7)\mu_B$ [Co(1)] and $3.84(5)\mu_B$ [Co(2)]. The absence of any anomaly in both the specific heat and thermal evolution of the magnetic moments below ~20 K confirms the blocking process of a spin glass behavior. The crystal-field splitting of the Co^{2+} ions causes a single ion anisotropy along the *z* (*c*-axis) direction, giving an Ising character in which the local spins from the Co(1) dimers are frozen. A magnetic frustration in the Co(1) magnetic moments is observed as due to the presence of antiferromagnetic interactions between Co(2) neighbor chains. It is to note the existence of a Co(1)-O(3)(PO_3)-Co(2) superexchange angle with a value of 107° that involves ferromagnetic couplings between chain and dimer neighbors ferromagnetically coupled. This exchange pathway together with the anisotropy and frustration could be the responsible of the spin glass behavior observed in the three-dimensional antiferromagnetic $Co_2(OH)(PO_4)$ ordered phase.

DOI: 10.1103/PhysRevB.66.094406 PACS number(s): 75.50.Lk, 61.12.−q

I. INTRODUCTION

The great ability of phosphate and arsenate frameworks to stabilize different oxidation states is produced for the relatively high charge in XO_4^{3-} tetrahedra that favors the formation of anionic frameworks with a high degree of mechanical, chemical, and thermal stability.[1,2] These compounds, minerals in some cases, offer a considerable number of structures which can give rise to original physical properties (magnetic, heterogeneous catalysis, ion exchange, optical, etc) with potential applications. Hydrothermal techniques can be used as an adequate synthetic method to prepare minerals or complex phosphates and arsenates of transition metals, where a systematic variation of the temperature and pressure can originate interesting structural phases.

The complex structural chemistry of minerals of formula $ABXO_4$ has been known for many years,[3] and several structural types have been elucidated for this general formula. The adamite-type $M_2(O/OH)(XO_4)$ family includes different phases such as $Zn_2(OH)(AsO_4)$ (adamite),[4] $Mn_2(OH)(AsO_4)$ (eveite),[5] $Cu_2(OH)(PO_4)$ (libethenite),[6] $Cu_2(OH)(AsO_4)$ (olivenite),[7] and Al_2OSiO_4 (andalusite).[8] In addition, the $Co_2(OH)(AsO_4)$ phase has been found in solid solution with adamite.[9] The crystal structure of $Co_2(OH)(PO_4)$ was recently published.[10] Unfortunately, even if good crystals for x-ray structure determination were obtained, powdered pure phases were not prepared. This fact precluded carrying out any study on the physical properties of this material. However, by changing the synthetic method and using mild hydrothermal reactions starting from a known precursor and checking the *p*H of the mixture reaction allowed us the attainment of $Co_2(OH)(PO_4)$ as a pure phase.

The crystal structure of $Co_2(OH)(PO_4)$ contains two different topologies for the metal ions, such as the octahedral and trigonal bipyramidal (Fig. 1). The $[Co(2)O_4(OH)_2]$ octahedron shares two opposite edges with two neighboring octahedra to form a linear chain propagated along the *c* axis. The two trigonal bipyramids $[Co(1)O_4(OH)]$ constitute a dimer by sharing an edge. The dimeric unit, the linear chain of the octahedra, and the anion tetrahedra share corners thereby forming a three-dimensional network. Considering the presence of two different metal positions together with

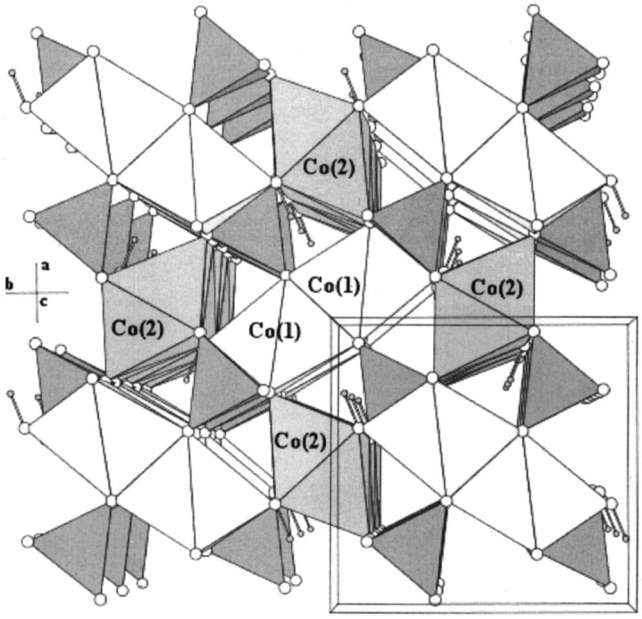

FIG. 1. Polyhedral view of the crystal structure of $Co_2(OH)(PO_4)$ in the [001] direction. Light and dark octahedra are occupied by the Co(1) and Co(2) ions, respectively. The PO_4 groups are represented by the dark tetrahedra. Open circles correspond to the oxygens atoms, and little circles show the hydrogen atoms.

the nature (anisotropy and spin-orbit coupling) of the Co^{2+} ions, interesting physical properties should be expected.

In this work we report, as far as we are aware, on the first ordered phosphate $Co_2(OH)(PO_4)$ with a spin-glass behavior. Spectroscopic and magnetic properties are discussed in order to investigate the nature of the anomalies showed by the magnetic measurements. Neutron powder diffraction experiments allow us to determine the magnetic structure of the low-temperature ordered phase. The thermal evolution of the magnetic moments suggests that below $\sim$20 K these are practically saturated.

II. EXPERIMENT

$Co_2(OH)(PO_4)$ was synthesized by mild hydrothermal conditions starting from the $Co_3(PO_4)_2 8H_2O$ phase, which was previously described.[11] Approximately 0.2 g of this precursor were disgregated in 35 mL of water and were placed in a poly(tetrafluoroethylene)-lined stainless steel container (fill factor 75%) under autogeneous pressure generated by a temperature of $\approx$180 °C for one week. The content of Co and P in the microcrystalline purple powdered sample was calculated by inductively coupled plasma atomic emission spectroscopy with an ARL Fisons 3410 spectrometer, confirming the $Co_2(OH)(PO_4)$ chemical formula.

An x-ray powder diffraction pattern was collected on a Philips X'PERT automatic diffractometer in Bragg-Brentano geometry operating at 40 kV and 40 mA. The Cu $K\alpha$ radiation ($\lambda = 1.5418$ Å) was employed with steps of 0.02° in 2θ and fixed time counting of 1 s in the $5° \leqslant 2\theta \leqslant 80°$ range. Neutron powder diffraction measurements were performed on the D1B and D2B powder diffractometers, at the Institute Laue-Langevin of Grenoble, using wavelengths of 2.52 and 1.595 Å, respectively. About 5.0 g of $Co_2(OH)(PO_4)$, contained in a cylindrical vanadium can and held in a liquid-helium cryostat, were employed in both experiments. The high resolution of D2B was used to obtain extensive and accurate structural data of cobalt hydroxyphosphate at room temperature, at 30 and 2 K, respectively, over a large angular angle $0 \leqslant 2\theta \leqslant 160°$. D1B has a 400-element linear multidetector covering an angular range of 80°. The high flux and medium resolution of D1B were used to study the thermal evolution of the sample, in the temperature range 1.7–150 K. The diffraction patterns were collected every 2 K for 5 min in the angular range $10 \leqslant 2\theta \leqslant 90°$. The Rietveld method[12] was used to refine the crystal and magnetic structures. All the data, from x-ray as well as from neutron diffraction, were analyzed with use of the FULLPROF (Ref. 13) program suite. For the patterns the backgrounds were fitted to a polynomial refinable function. The D1B patterns were refined sequentially, taking as starting parameters of each pattern those resulting from the refinement of the proceeding one. A pseudo-Voigt function was chosen to generate the line shape of the diffraction peaks. The structure determined by using x-ray single crystal data[10] was used as a starting model for the refinements.

Spectroscopic measurements were studied by both diffuse reflectance and electron paramagnetic resonance. The UV-visible spectrum was collected on a Cary 2415 spectrometer and registered at room temperature in the 5000–50 000-cm^{-1} range. The EPR measurements were recorded on a Bruker ESP 300 spectrometer at 4.2 K. The temperature was stabilized by an Oxford Instrument (ITC4) regulator. The magnetic field was measured with a Bruker BNM 200 gaussmeter, and the frequency inside the cavity was determined using a Hewlett Packard 5352B microwave frequency counter.

Magnetic susceptibility measurements (dc) were performed in an applied field of 0.1 T over the temperature range $4.2 \leqslant T/K \leqslant 300$ using a Quantum Design MPSM-7 superconducting quantum interferency device magnetometer. Data were collected after both zero field cooling and field cooling of the sample. Magnetization was measured as a function of field in the range $-7 \leqslant H/T \leqslant 7$ at a temperature range after cooling the sample in a zero field. For the ac magnetic susceptibility, we used a standard quantum dot PPMS system with an alternate excitation field of 1 Oe and frequencies between 10 and 10^4 Hz. Heat capacity measurements were also carried out by a relaxation method, also using a PPMS system. The sample was a plate of 0.3-mm thickness and 7-mg weight, obtained by compressing the original powder.

III. RESULTS

A. Room-temperature structure

The x-ray powder diffraction data were used to evaluate the purity of the product obtained in the synthesis. The data were fitted using the pattern matching routine of the program FULLPROF,[13] in the *Pnnm* space group with the cell parameters reported by Harrison *et al.*[10] (from single-crystal data) as starting point. No extra diffraction peaks were observed in

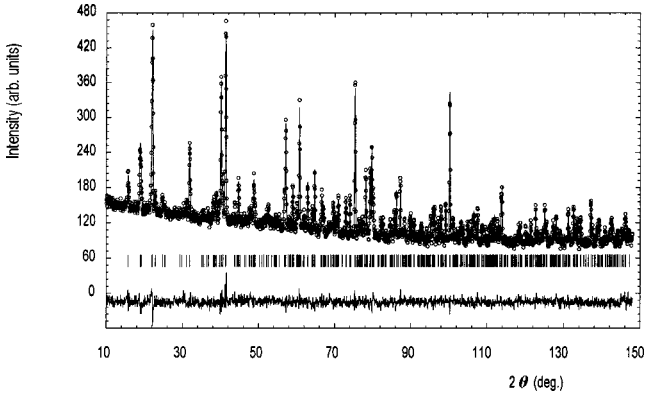

FIG. 2. Observed (crosses), calculated (solid line), and difference (at the bottom) neutron diffraction (D2B, ILL) profiles of $Co_2(OH)(PO_4)$ at room temperature. Vertical marks correspond to the position of the allowed reflections for the crystallographic structure.

the final refinement, concluding that the compound obtained corresponds to a pure phase. The x-ray refined unit-cell parameters are $a=8.043(1)$, $b=8.380(1)$, and $c=5.953(1)$ Å, very close to those reported in Ref. 10: $a=8.042(3)$, $b=8.369(2)$, and $c=5.940(2)$ Å.

The room-temperature D2B powder neutron diffraction pattern was refined using the Rietveld method taking as starting model the $Co_2(OH)(PO_4)$ crystal structure reported in Ref. 10. The experimental, calculated and difference neutron powder diffraction profiles for $Co_2(OH)(PO_4)$ are shown in Fig. 2. The room-temperature structural parameters and the reliability factors from D2B data refinement are summarized in Table I.

The final refined positional and thermal parameters are given in Table II: As can be seen two independent crystallographic sites for cobalt and one for phosphorus are present in the compound. The main interatomic distances and angles for the cobalt hydroxyphosphate compound are listed in Table III.

B. Spectroscopic measurements

The diffuse reflectance spectrum of $Co_2(OH)(PO_4)$ shows the spin-allowed transitions of the CoO_6 octahedral chromophore, ${}^4T_{1g}\rightarrow{}^4T_{2g}$, ${}^4A_{2g}$, and ${}^4T_{1g}(P)$ at the frequencies 8450, 15 450, and 18 350 cm^{-1}, respectively. The Dq and the B Racah parameters, calculated by fitting the experimental frequencies to an energy-level diagram for an octahedral d^7 system,[14] are 720 and 875 cm^{-1}, respectively. Other bands at frequencies of 6400, 7000, 11 100, 15 800, and 19 600 cm^{-1} were also observed. These bands were attributed to the ${}^4A_2'\rightarrow{}^4A_1''$, ${}^4A_2''$; ${}^4E''$; ${}^4E'$; ${}^4A_2'(P)$, and ${}^4E''(P)$ spin-allowed transitions of the CoO_5 trigonal bipyramid chromophore.

The EPR spectroscopy also indicates the presence of the octahedral CoO_6 and trigonal bipyramidal CoO_5 symmetries in this compound. In order to obtain a good resolution of the EPR spectrum we doped 0.1% Co in a matrix of $Zn_2(OH)(PO_4)$ which is isoestructural with the cobalt phase. The spectrum at 4.2 K is shown in Fig. 3(a). It can be described in terms of a spin doublet $S=\frac{1}{2}$ interacting with a single ^{59}Co nucleus ($I=\frac{7}{2}$) as it is simulated in the theoretical EPR spectrum of Fig. 3(b). This effective spin doublet arises from the splitting of the ${}^4T_1$ term through spin-orbit coupling and local distortion of the octahedral sites.[15] It shows the strong anisotropy of the g factor and hyperfine coupling constant characteristic of Co^{2+} ions in distorted octahedral environments. The g values obtained are $g_1=5.890$, $g_2=4.550$, and $g_3=2.021$. The observed value for the sum of the three orthogonal g values ($g_s=12.46$) is in good agreement with the theoretical value near 13 proposed by Abragam and Pryce.[16] The hyperfine splitting parameters $A_1=240\times10^{-4}$ cm^{-1}, $A_2=155\times10^{-4}$ cm^{-1}, and $A_3=85\times10^{-4}$ cm^{-1} are similar in magnitude to those observed in $Mg_2(OH)(AsO_4)$ doped with Co^{2+} and other related Co(II) compounds,[17–20] with six O^{2-} ions as the nearest neighbors of Co^{2+}.

TABLE I. Details of full-profile refinements from neutron-diffraction pattern at room temperature for $Co_2(OH)(PO_4)$. Single-crystal unit-cell parameters from Ref. 10: $a=8.042(3)$ Å, $b=8.369(2)$ Å, $c=5.940(2)$ Å, and $V=399.8$ $Å^3$.

Compound	$Co_2(OH)PO_4$
Space group	*Pnnm* (No. 58)
a (Å)	8.040(1)
b (Å)	8.376(1)
c (Å)	5.951(1)
V ($Å^3$)	399.8(1)
Instrument	D2B (ILL)
Radiation (Å)	1.594
Monochromator	Ge (335)
Z	4
2θ range (°)	0–160
2θ step-scan increment (°)	0.05
No. of reflections	444
No. of profile parameters	35
Reliability factors (%):	
$R_P=\Sigma\lvert y_{i,\mathrm{obs}}-(1/c)y_{i,\mathrm{calc}}\rvert/\Sigma y_{i,\mathrm{obs}}$	3.69
$R_{\mathrm{WP}}=[\Sigma w_i\lvert y_{i,\mathrm{obs}}-(1/c)y_{i,\mathrm{calc}}\rvert^2/\Sigma w_i[y_{i,\mathrm{obs}}]^2]^{1/2}$	4.62
$R_B=[\Sigma\lvert I_{\mathrm{obs}}-I_{\mathrm{calc}}\rvert]/\Sigma I_{\mathrm{obs}}$	10.1
χ^2	1.27

TABLE II. Final refined positional and thermal parameters from the neutron-diffraction pattern (D2B) at room temperature for $Co_2(OH)(PO_4)$.

Atom	x/a	y/b	z/c	B ($Å^2$)
Co(1)	0.360(1)	0.364(1)	0.5	0.6(1)
Co(2)	0.5	0	0.252(1)	0.6(1)
P(1)	0.2476(7)	0.2405(5)	0	0.9(7)
O(1)	0.1083(6)	0.1135(5)	0	0.90(3)
O(2)	0.4139(4)	0.1470(6)	0	0.90(3)
O(3)	0.2318(4)	0.3472(3)	0.2098(4)	0.90(3)
O(4)	0.3821(6)	0.1244(5)	0.5	0.90(3)
H(1)	0.274(1)	0.0809(9)	0.5	2.1(1)

TABLE III. Main interatomic distances (Å) and angles (°) for $Co_2(OH)(PO_4)$ (D2B, RT). Symmetry code: $i=\frac{1}{2}-x,\ y-\frac{1}{2},\ \frac{1}{2}-z;\ ii=\frac{1}{2}-x,\ \frac{1}{2}+y,\ \frac{1}{2}-z;\ iii=x-\frac{1}{2},\ \frac{1}{2}-y,\ z-\frac{1}{2};\ iv=-x,\ -y,\ 1-z;\ v=x-\frac{1}{2},\ \frac{1}{2}-y,\ \frac{1}{2}-z;\ vi=-x,\ -y,\ -z;\ vii=x,\ y,\ -z;\ viii=x,\ y,\ 1-z.$

BOND DISTANCES (Å)			
$Co(2)O_4(OH)_2$		$Co(1)O_4(OH)$	
Co(2)-O(2)	2.062(9)×2	Co(1)-O(4)H	2.02(1)
Co(2)-O(4)H	2.038(8)×2	Co(1)-O(1)^{ii}	2.09(1)
Co(2)-O(3)^{i}	2.272(3)×2	Co(1)-O(1)^{iii}	2.00(1)
		Co(1)-O(3)	2.019(5)×2
PO_4			
P-O(1)	1.544(7)		
P-O(2)	1.549(7)		
P-O(3)	1.540(4)×2		
BOND ANGLES (°)			
$Co(2)O_4(OH)_2$		$Co(1)O_4(OH)$	
O(2)-Co(2)-O(2)	86.4(4)	O(1)H-Co(1)-O(1)^{iii}	77.9(4)
O(2)-Co(2)-O(3)H	97.6(3)×2	O(1)H-Co(1)-O(3)	97.6(4)×2
O(2)-Co(2)-O(3)^{v}	90.6(3)×2	O(1)^{ii}-Co(1)-O(4)^{iii}	168.2(5)
O(2)-Co(2)-O(4)^{i}	171.0(4)×2	O(1)^{iii}-Co(1)-O(3)	121.1(4)×2
O(3)H-Co(2)-O(3)H^{vi}	168.6(2)	O(3)^{ii}-Co(1)-O(4)	88.3(4)×2
O(3)H-Co(2)-O(4)^{i}	80.5(3)×2		
O(3)H-Co(2)-O(4)^{v}	91.2(3)×2		
O(4)^{i}-Co(2)-O(4)^{v}	171.0(4)		
PO_4			
O(1)-P-O(2)	106.1(5)		
O(1)-P-O(3)	109.8(4)×2		
O(2)-P-O(3)	111.3(4)×2		
O(3)-P-O(3)^{viii}	108.3(3)		

Furthermore, other weak absorption bands were also observed in the EPR spectrum, at around 210 mT, which can be attributed to a small portion of Co(II) ions placed in the trigonal bipyramidal positions of the crystal structure. The g values corresponding to this symmetry were determined in a complete EPR study of the $Zn_2(OH)(PO_4)$: 0.1%Co and other hydroxiarsenate −Co(II) compounds.[21] In this work a spin doublet $S=\frac{1}{2}$ was also found as the ground state when the crystal field of the trigonal bipyramidal together with the spin-orbit interactions are considered.

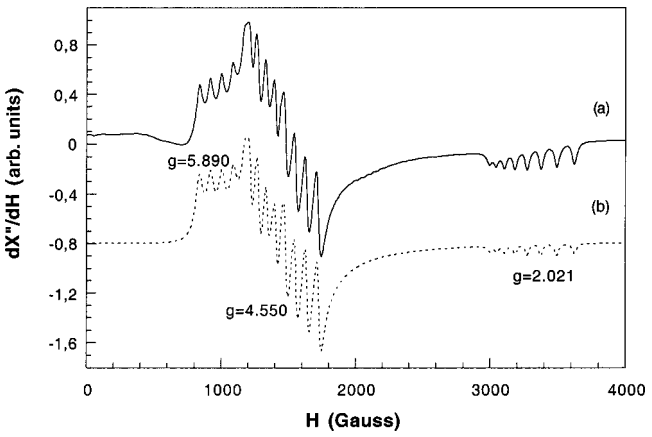

FIG. 3. Experimental (a) and simulated (b) EPR powder spectra of Co^{2+} in $Zn_2(OH)(PO_4)$ at 4.2 K.

C. Magnetic properties

Variable temperature magnetic susceptibility measurements of $Co_2(OH)(PO_4)$ have been carried out on a powdered sample in the 4.2–300-K temperature range. Figure 4 shows the temperature dependence of the magnetic and reciprocal susceptibilities. At high temperatures ($T>100$ K) the thermal evolution of χ_m follows a Curie-Weiss law, $\chi=C/(T-\theta)$, with $C_m=3.59\ cm^3\ K/mol\ Co^{2+}$ and $\theta=-63.5$ K. The molar magnetic susceptibility increases from room temperature with decreasing temperature and reaches a first maximum at circa 70 K, indicating that a long magnetic order is established at this temperature. At low temperatures ($T<20$ K) other strong magnetic signal centered at 13 K appears (see Fig. 4). The negative Weiss constant together with the continuous decrease in the $\chi_m T$ vs T curve, from

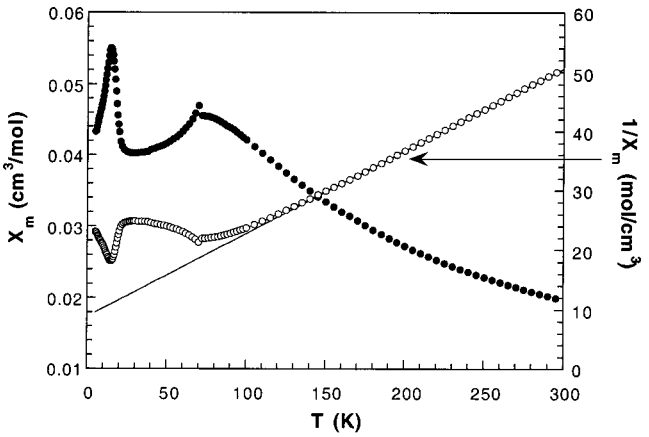

FIG. 4. Thermal evolution of the molar magnetic susceptibility (χ_m) and inverse susceptibility ($1/\chi_m$) for $Co_2(OH)(PO_4)$.

$5.9\mu B$ at room temperature to $0.2\mu B$ at 4.2 K, imply that the dominant interactions between neighboring Co(II) ions are antiferromagnetic.

Thermoremanent magnetization (TRM), as a function of temperature, between 4.2 and 100 K, is given in Fig. 5(a). The TRM curve was measured at $H=0$ after cooling from $T>T_N$ under a magnetic field of 0.1 T. Its value decreases by increasing the temperature up to 7 K where an up turn is observed. After a small maximum at $T=13$ K ($Mr \approx 35$ emu/mol) the TRM strongly decreases and then, between 20 and 50 K the remanent magnetization was practically constant with a value of 5 emu/mol. By increasing the temperature above 70 K, the remanent magnetization reduces to zero, as corresponds to a paramagnetic state. The existence of a remanent magnetization different from 0 below 70 K reflects the existence of a ferromagnetic component, which is larger below 20 K. In fact, the magnetization variation with the magnetic field at $T=15$ K shows a small hysteresis loop in which the *Hc* and *Mr* values are 25 G and 9 emu/mol, respectively [see Fig. 5(b)]. At this temperature the saturation is not reached. Below 15 K the observed hysteresis loop is less than that of 15 K with relatively small coercitivity commonly observed in spin glasses[22] [see the inset in Fig. 5(b)].

The results of the magnetization at low fields, measured warming under 0.1 T after cooling down from room temperature first without an applied field [zero field cooled (ZFC)] and subsequently under applied field [field cooled (FC)], are shown in Fig. 6. The low-temperature behavior is characterized by a sharp maximum in the ZFC-FC signals at 13 K. Magnetic irreversibility can be observed below this temperature being the magnetization measured after cooling the sample in the applied field (FC) constant down to 7 K. At temperatures higher than 15 K no difference between ZFC and FC magnetization is observed. The magnetic irreversibility is lower for an applied magnetic field of 1 T (see the inset of Fig. 6). The effect of irreversibility observed in the magnetization curves is characteristic of a spin-glass-like behavior.

ac measurements are given in Fig. 7. The real (χ') and imaginary (χ'') components of the susceptibility at 100 Hz

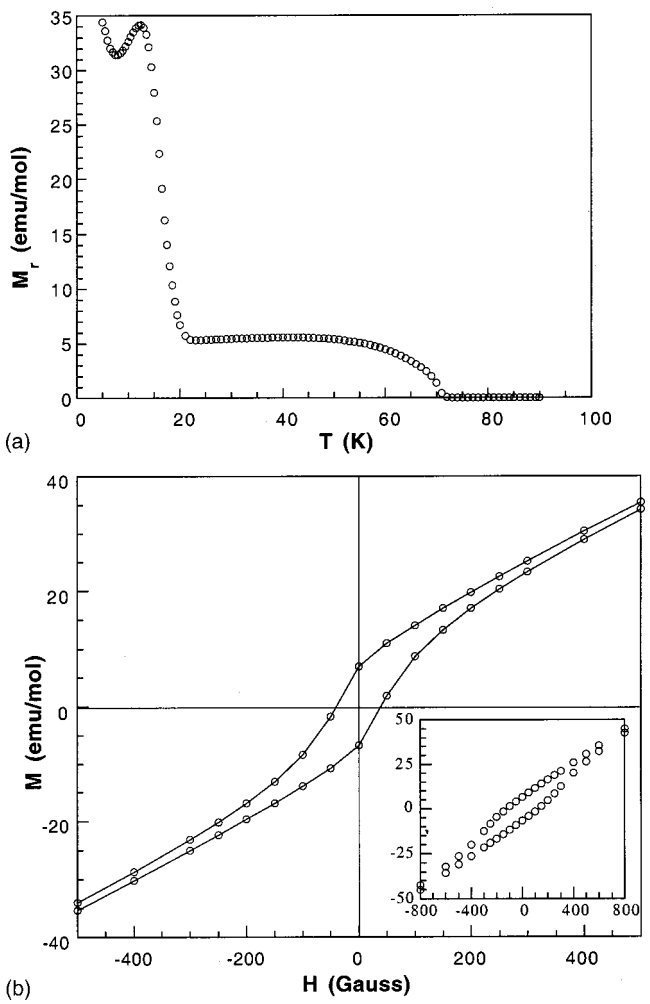

FIG. 5. (a) Temperature dependence of the magnetization between 4.2 and 100 K for $Co_2(OH)(PO_4)$. (b) Magnetization vs. applied magnetic field at 15 K. The inset shows the measurements at 10 K.

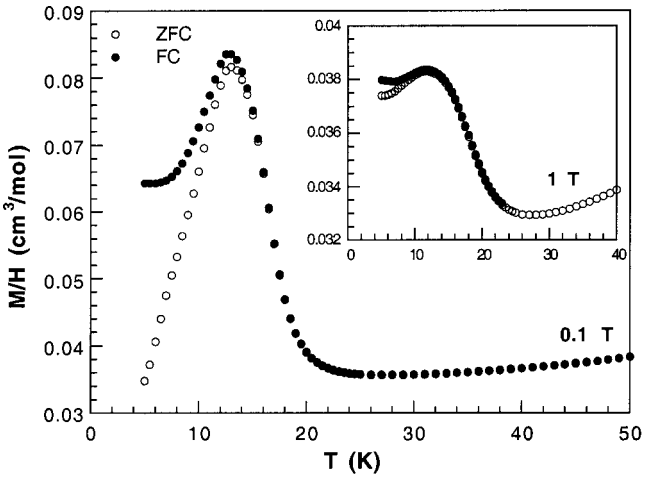

FIG. 6. Low field ZFC-FC magnetization of the $Co_2(OH)(PO_4)$ showing the blocking process at $T=13$ K taken at an applied field of 0.1 T. The inset shows the measurements at 1 T.

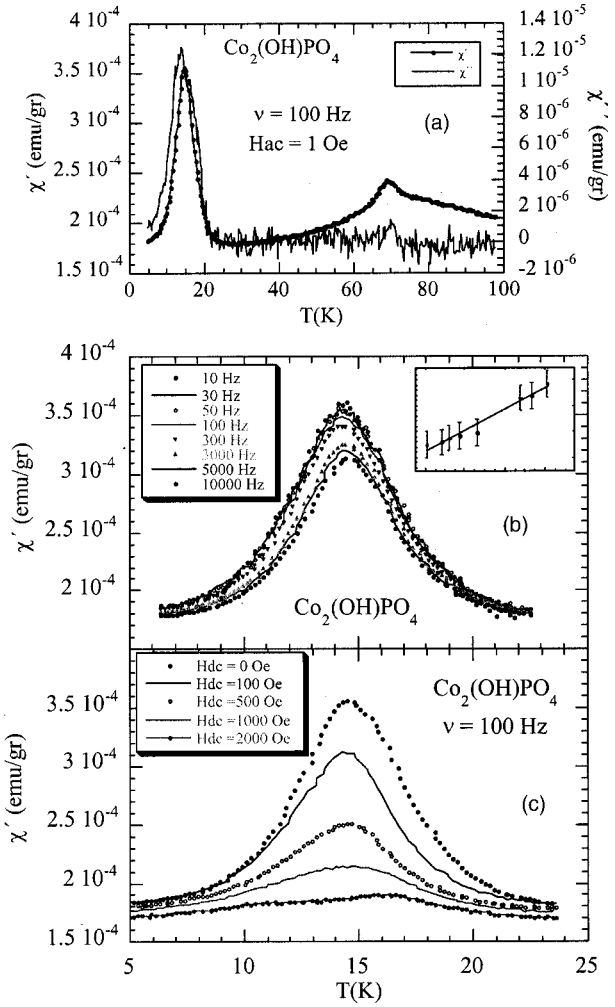

FIG. 7. Evolution with temperature of the ac susceptibility of $Co_2(OH)PO_4$ measured with an ac applied field $H_{ac}=1$ Oe (a) In phase (χ') and out-of-phase phase (χ'') susceptibilities at a frequency $\nu=100$ Hz. (b) χ' susceptibility curves at different excitation frequencies. The inset show the evolution of the maximum's temperature with frequency; see the text. (c) χ' susceptibility curves under different dc applied fields.

with an ac field of 1 Oe are shown in Fig. 7(a). The maximum observed at 70 K in the (χ') measurements is associated with the long-range order interactions. The lack of absorption in out-of-phase (χ'') ac susceptibility in this temperature region indicates the presence of antiferromagnetic order, in good agreement with the results obtained from χ_m vs T. Strong peaks are observed in both χ' and χ'' at around 15 K indicating the presence of a magnetic transition of different nature than the previous one. A detailed analysis of the ac susceptibility has been performed around this temperature. The ac susceptibility curves were measured at different frequencies [see Fig. 7(b)]. The values are independent of the frequency up to the proximities of the maximum which is frequency dependent. The peak height decreases and the position of the maximum shifts to higher temperatures with increasing frequency. The influence of a superposed dc field was also studied [Fig. 7(c)]; the ac susceptibility shows a strong dependence on magnetic field, and the

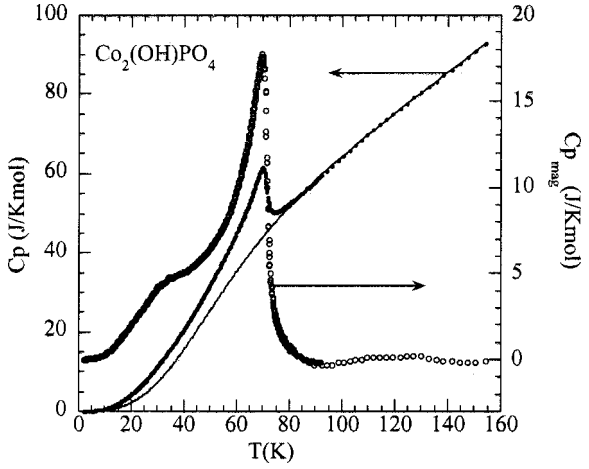

FIG. 8. Specific heat of $Co_2(OH)PO_4$ between 1.8 and 150 K. Experimental data (full points), estimated phonon contribution (full line), and magnetic contribution (circles).

peak nearly disappears under an applied magnetic field of 2000 Oe. These dependences are consistent with a cooperative freezing of individual magnetic moments, as occur in spin glasses, the freezing temperature T_f being defined as that corresponding to the maximum in χ'.

The specific-heat data between 1.8 and 150 K are shown in Fig. 8. The heat-capacity measurements exhibit a three-dimensional magnetic ordering peak at 70 K. The temperature at which this (λ-type) peak appears is nearly the same to that obtained from the magnetic susceptibility measurements ($T\approx 70$ K). The strong increase of Cp at higher temperatures is due to the lattice contribution (Cp_{pho}). The high temperature of the λ-type peak does not permit to calculate the magnetic contribution (Cp_{mag}) in a accuracy way. This contribution is relatively important compared with the phonon one at low temperatures. However, the phonon contribution at around the magnetic transition (70 K) is approximately four times larger. We tried to estimate Cp_{pho} by fitting the experimental data above the λ-type anomaly to the Debye model; however, a large difference between both the theoretical and experimental data was observed. The reason of such discrepancy can be attributed to the presence in the unit cell of atoms such as Co and P with higher masses than those of the O and H atoms. Therefore, more than one phonon spectrum can be present in the compound. We intended to determine Cp_{pho} from a theoretical method using the Debye model which usually best follow Cp_{pho} in a wide temperature range. In this framework, the simplest model is to consider the existence of two different phonon spectra. In this way, if the number of atoms in the unit cell is N, we suppose n_1 atoms with a Debye temperature θ_1 and $n_2=(N-n_1)$ atoms with a Debye temperature θ_2. Therefore, there are three free parameters, namely, n_1, θ_1, and θ_2. The best fitting is obtained for $n_1=5.8$, $\theta_1=1141$ K, and $\theta_2=267$ K. The good quality of the fit (see the continuous line in Fig. 8) as well as the meaning of the obtained values [the number of ions associated with the largest Debye temperature are nearly the number of the lighter ions (6)] allow us to consider that this phenomenological model determine reasonable well the pho-

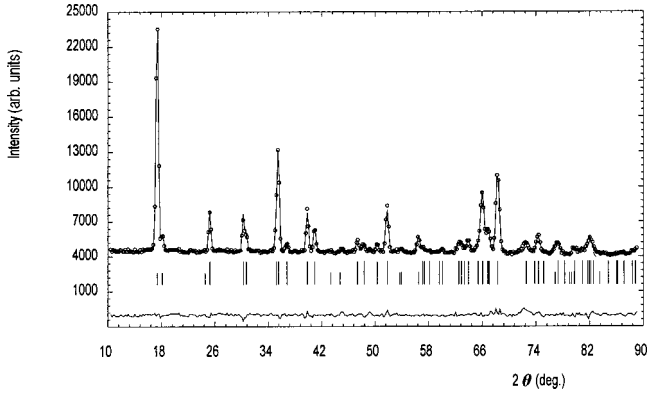

FIG. 9. Refinement (D1B) of the $Co_2(OH)(PO_4)$ neutron-diffraction profile at 2 K (the intensity is in arbitrary units). The position of the Bragg reflections for the crystallographic (first row) and magnetic (second row) structures are presented. The difference curve is plotted at the bottom of the figure.

non contribution. The magnetic contribution was calculated as $Cp_{\mathrm{mag}}=Cp-Cp_{\mathrm{pho}}$ (see Fig. 8). In addition to the λ-type peak at the ordering temperature, we can also observe the existence of a shoulder at around 30 K which can be attributed to a spin glass-like behavior where a broad anomaly in Cp_{mag} usually appears at temperatures higher than the freezing one.

D. Low-temperature neutron diffraction

1. Magnetic structure refinements

The low-temperature D2B diffraction patterns were collected at 30 and 2 K below the first and second magnetic transitions, respectively. Both patterns exhibit extra magnetic peaks indicating that $Co_2(OH)(PO_4)$ is magnetically ordered at these temperatures. Extra diffraction peaks were clearly observed in the neutron pattern at 30 K with a very intense magnetic reflection at $d=8.36$ Å. Nevertheless, no new extra magnetic contributions are observed at 2 K indicating the absence of either a new or different magnetic ordering at this temperature, in good agreement with the magnetic data. The D1B diffraction pattern at 1.5 K shows a better resolution of the magnetic reflection at $d=8.36$ Å, indicating the existence of two resolved magnetic peaks in this angular range (see Fig. 9). All magnetic peaks can be indexed with a propagation vector $k=(0,0,0)$ referring to the room-temperature (RT) unit cell, indicating that both the magnetic and nuclear unit cells are similar.

The possible magnetic structures compatible with the *Pnnm* crystal symmetry has been evaluated with the help of Bertaut's macroscopic theory[23] that allows one to determine the symmetry constraints between each magnetic moment of Co^{2+} belonging to the same general crystallographic position. The magnetic atoms occupy two different special sites. Co(1) atoms (named *R*) are in a $4g$ position and are numbered (1) $x, y, \frac{1}{2}$; (2) $-x, -y, \frac{1}{2}$; (3) $1/2+x, 1/2-y, 0$; (4) $1/2-x, 1/2+y, 0$. Co(2) atoms (named *S*) in a $4f$ position and are numbered (1) $\frac{1}{2}, 0, z$; (2) $\frac{1}{2}, 0, -z$; (3) $0, \frac{1}{2}, 1/2+z$; (4) $0, \frac{1}{2}, 1/2-z$. The Ri and Si atoms from the two sublattices are present in the crystal structure. In the unit cell two dimers ($R1-R2$ and $R3-R4$) and two chains ($-S1-S2-$ and $-S4-S3-$) are present. Using the method developed by Bertaut and taking into account the restrains imposed by the independent symmetry elements of the space group *Pnnm* along the three directions *x*, *y*, and *z*, the possible orientations of the magnetic moments in every sublattice were calculated. The agreement between the observed and calculated diffraction patterns for each possible magnetic structure has been tested. The best agreement was obtained with the magnetic

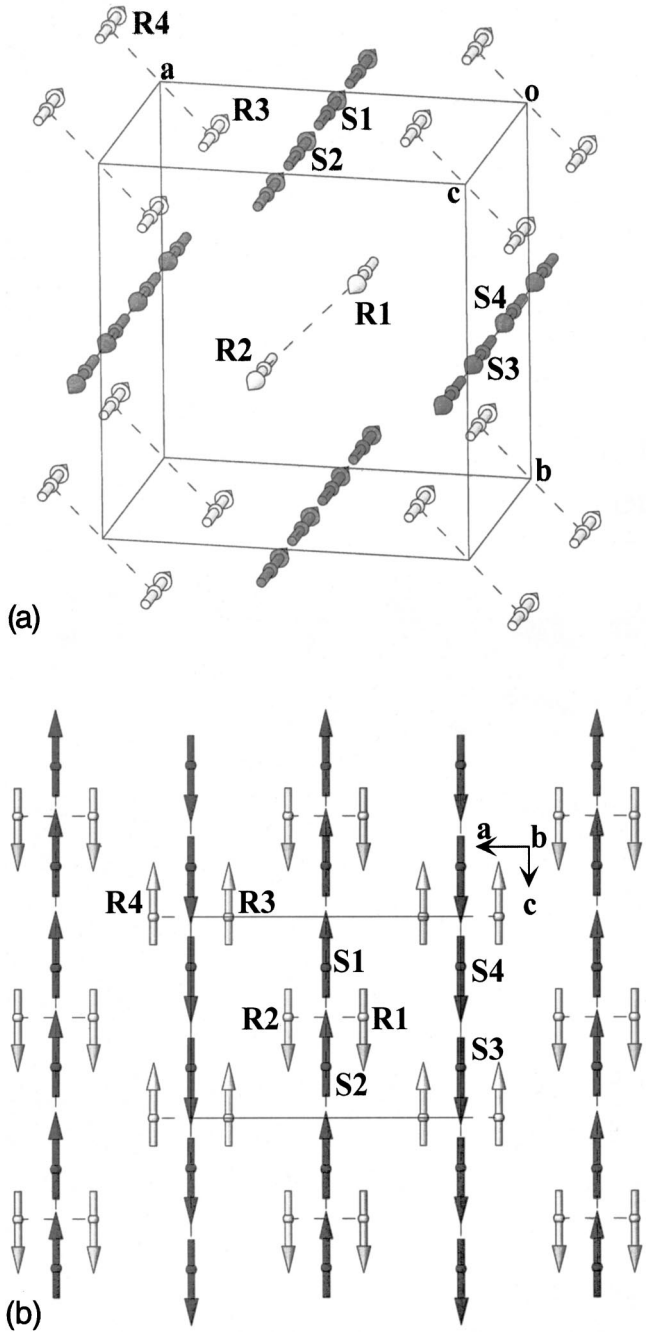

FIG. 10. Projection of the magnetic structure onto the bc plane. Black and white spheres representing the two types of Co crystallographic ions (sublattices *R* and *S*). The directions of the electronic spins in the *z* axis are marked.

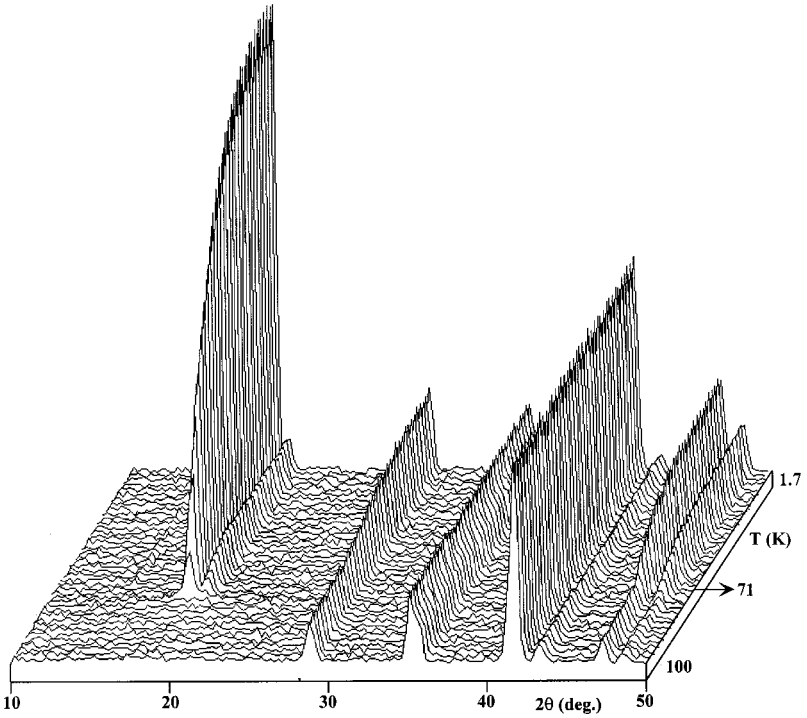

FIG. 11. Thermal evolution of the neutron-diffraction patterns of $Co_2(OH)(PO_4)$.

moments in the *z* direction.

In the case of the *R* sublattice [Co(1)], the relationship between the magnetic moments is $+R1z+R2z$ and $-R3z-R4z$. For the *S* sublattice [Co(2)] the relationship is $-S1z-S2z$ and $+S4z+S3z$. The best fit of the D1B experimental pattern at 1.5 K is plotted in Fig. 9. The saturated magnetic moments of Co(1) and Co(2) are respectively $m_z=3.39(7)\ \mu B$ and $m_z=3.84(5)\ \mu B$ per cobalt ion. The nuclear and magnetic discrepancy factors are $R_p=1.88$, $R_{wp}=2.49$, $\chi^2=3.19$, $R_{Bragg}=7.35$, and $R_{mag}=7.27$.

The representation of the magnetic structure of $Co_2(OH)(PO_4)$ is shown in Fig. 10. As previously indicated, the crystal structure consists of an arrangement of two types of entities linked by (PO_4) tetrahedra sharing the corners: Co(1) trigonal bipyramidal dimers (sublattice *R*) and Co(2) octahedral chains (sublattice *S*) parallels to the *z* direction [see Fig. 10(a)]. In the magnetic structure both entities are ferromagnetic along the *z* direction. In the *xz* plane the dimers and chains are ferromagnetically coupled [Fig. 10(b)], generating layers in which the magnetic moments are parallel. There are two types of ferromagnetic layers placed in the unit cell, at $y=0$ and 1/2, with their magnetic moments disposed antiparallel between them stabilizing the three-dimensional antiferromagnetic order through $|OH|$ and $|PO_4|$ groups. Although the refined model is overall antiferromagnetic, the arrangement of the magnetic moments allows the existence of a strong ferromagnetic component in the *z* direction. The values of the magnetic moments along the *x* and *y* directions were in the error limit of the measurements and were considered as negligible in the following refinements.

2. Thermal evolution of the ordered magnetic moments

The thermal evolution of the D1B neutron diffraction patterns for $Co_2(OH)(PO_4)$ from 1.7 to 100 K is shown in Fig. 11. The extra magnetic peaks appear below 71 K, which can be attributed to a three-dimensional antiferromagnetic ordering in the sample. The intensity of the magnetic reflections increases up to reach a maximum at around 40 K. Below this temperature the intensity is maintained constant up to 1.7 K.

The dependence of the lattice parameters and volume with temperature is shown in Fig. 12. The thermal expansion of the lattice parameters in the temperature range 1.7–150 K is anisotropic. The *b* parameter exhibits a great dispersion but the tendency of the values is practically constant. The *a* and *c* parameters show different behaviors with temperature: (i) Above 70 K, which is the temperature near the three-dimensional magnetic ordering, the *a* and *c* parameters show a positive dependence on temperature. (ii) Between 70 and 20 K the *a* parameter decreases with decreasing temperature whereas the *c* parameter shows a negative dependence with temperature. (iii) Below 20 K, where the spin glass behavior is evidenced, it can be surprisingly observed that the *a* parameter slightly increases up to 1.7 K. In the case of the *c* parameter the same tendency is followed in this temperature range. Finally, the thermal evolution of the unit cell volume indicates a slowly decrease up to 20 K followed by an increase below this temperature which can be attributed to the competition of the increasing and decreasing trends of the *a* and *c* parameters.

The thermal dependence of the ordered magnetic moments is represented in Fig. 13. It can be observed that the three-dimensional magnetic order begins at 71 K being the ordering temperature similar in both sublattices (see Figs. 11 and 13). The curves of the Co(1) and Co(2) moments rapidly increase from 70 to approximately 50 K with a change in the slope at around 40 K. The magnetic moment for Co(2) ions in the chains slowly increases with practically linear variation from $3.54(3)\mu_B$ at 50 K to $3.84(4)\mu_B$ at 2 K, reaching a saturation value at around 14 K. For the Co(1) ions in the

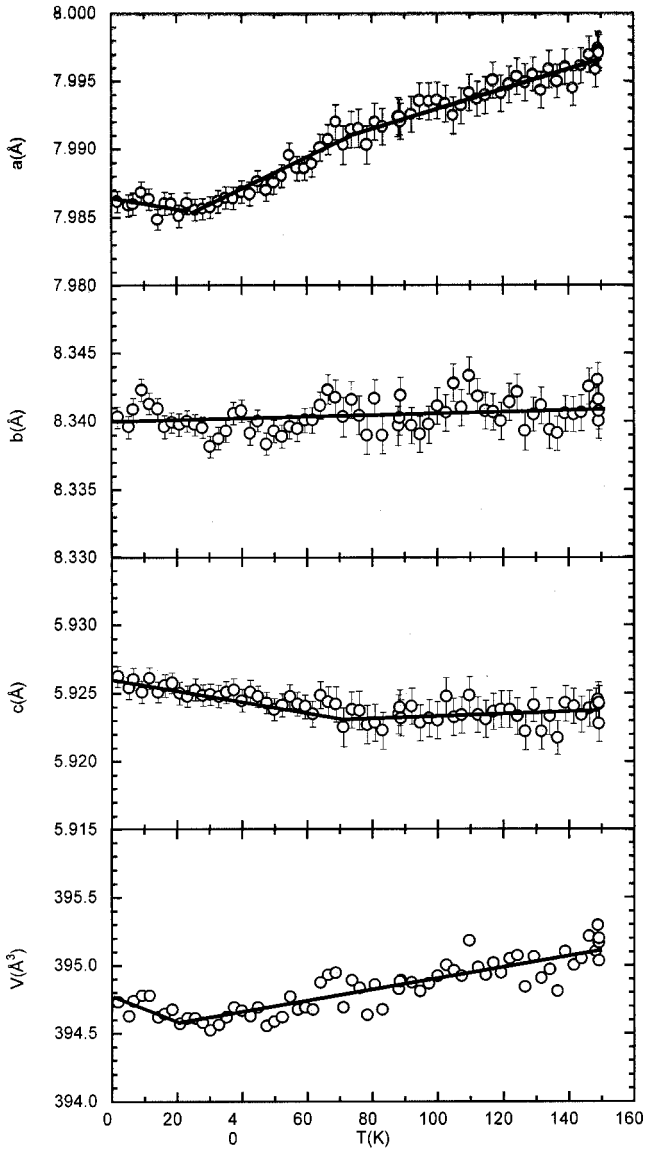

FIG. 12. Refined cell parameters and volume for $Co_2(OH)(PO_4)$ vs temperature from the D1B data between 1.7 and 150 K. Solid lines are only guides for the eye.

dimer groups, the magnetic moment increases more quickly from $2.65(5)\mu_B$ at 50 K to $3.39(5)\mu_B$ close to 6 K where the saturation value is reached (see Fig. 13). Furthermore, the refined magnetic moments of the Co(2) octahedral ions are always higher than those of the Co(1) bipyramidal trigonal geometry in all temperature ranges studied. The observed differences can be attributed to the distinct crystal effects[21] in both sublattices together with the presence of the spin glass state.

IV. DISCUSSION AND CONCLUSIONS

The ^4F ground state of isolated Co^{2+} $(3d^7)$ in a purely octahedral crystal field splits into two orbital triplets $^4T_1$, $^4T_2$, and one orbital $^4A_2$. Spin-orbit effects partially lift the degeneracy of the $^4T_1$ triplet into one Γ_6 subspace, two Γ_8 subspaces, and one Γ_7 subspace, and the resonance for the

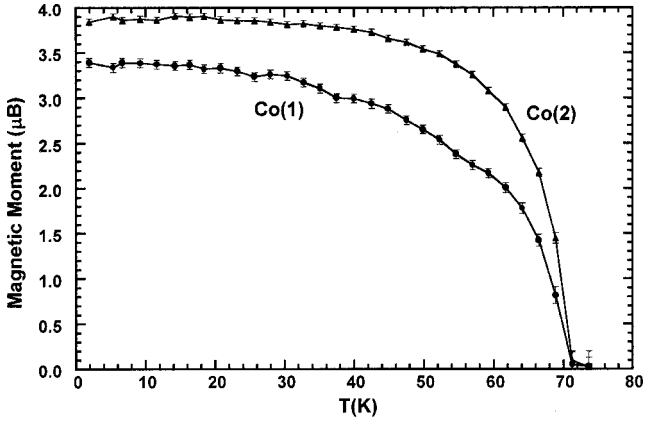

FIG. 13. Thermal evolution of the ordered magnetic moments of Co(1) and Co(2) ions in $Co_2(OH)(PO_4)$.

lowest doublet (Γ_6) is isotropic with $g=4.33$.[24] The addition of lower-symmetry crystal fields produces a further splitting of the $^4T_1$ triplet, giving six Kramer's doublets, and in most cases it is found that the trace of the g tensor is close to the cubic isotropic value;[25] in the present case the average g is 4.154. To understand this value we first consider the Co^{2+} ions in a cubic symmetry do not change this value in our approximation.

In the lower order one obtains g from the matrix elements of the Zeeman term in the Γ_6 subspace of the $^4T_1$ ground triplet. The matrix elements of the orbital angular momentum L within a T_1 subspace are proportional to those of a P term, but one should note that the excited term ^4P is also of the $^4T_1$ symmetry, and is mixed by the cubic field with the $^4T_1$ of the ground ^4F term. If we indicate two states of ^4F and ^4P with ϕ_i and ϕ_i', respectively, such that they transform in the same way under the cubic group, the states of the ground $^4T_1$ will be of the form $a\phi_i+b\phi_i'$.[26] The values of the constants a and b can be obtained[26,27] from the Racah parameter B, and the crystal-field parameter Dq, that take the values 875 and 720 cm^{-1}, respectively, in the $Co_2(OH)(PO_4)$ compound. With these values one obtains $a=-0.9820$ and $b=0.1886$, and the proportionality constant of the angular momentum is $\alpha=-1.5a^2+b^2=-1.4110$. Two further effects should be considered in the calculation of the isotropic_g_tensor. One is the second-order contribution of the $^4T_2$ states, that are separated by $\Delta'=-15B-6Dq=7000\ cm^{-1}$ from the ground $^4T_1$ states, and the other is the covalency between the Co and the neighboring O, described by several covalence factors,[25,26] that reduce the matrix elements of the orbital angular momentum and of the spin-orbit interaction. Using a single k_o for all these factors one obtains the expression for the g factor in a cubic field,

$$g=\frac{5}{3}g_e-\frac{2}{3}\alpha k_o+2\left(\frac{\sqrt{15}}{2}a+b\right)^2(k_o)^2\frac{|\lambda|}{\Delta'}, \qquad (1)$$

where $\lambda=-180\ cm^{-1}$ is the Co^{2+} spin-orbit interaction. With the parameters employed, this isotropic g tensor coincides with the trace of the experimental one when $k_o=0.86$. When one employs the parameters of Co MgO,[24] viz.

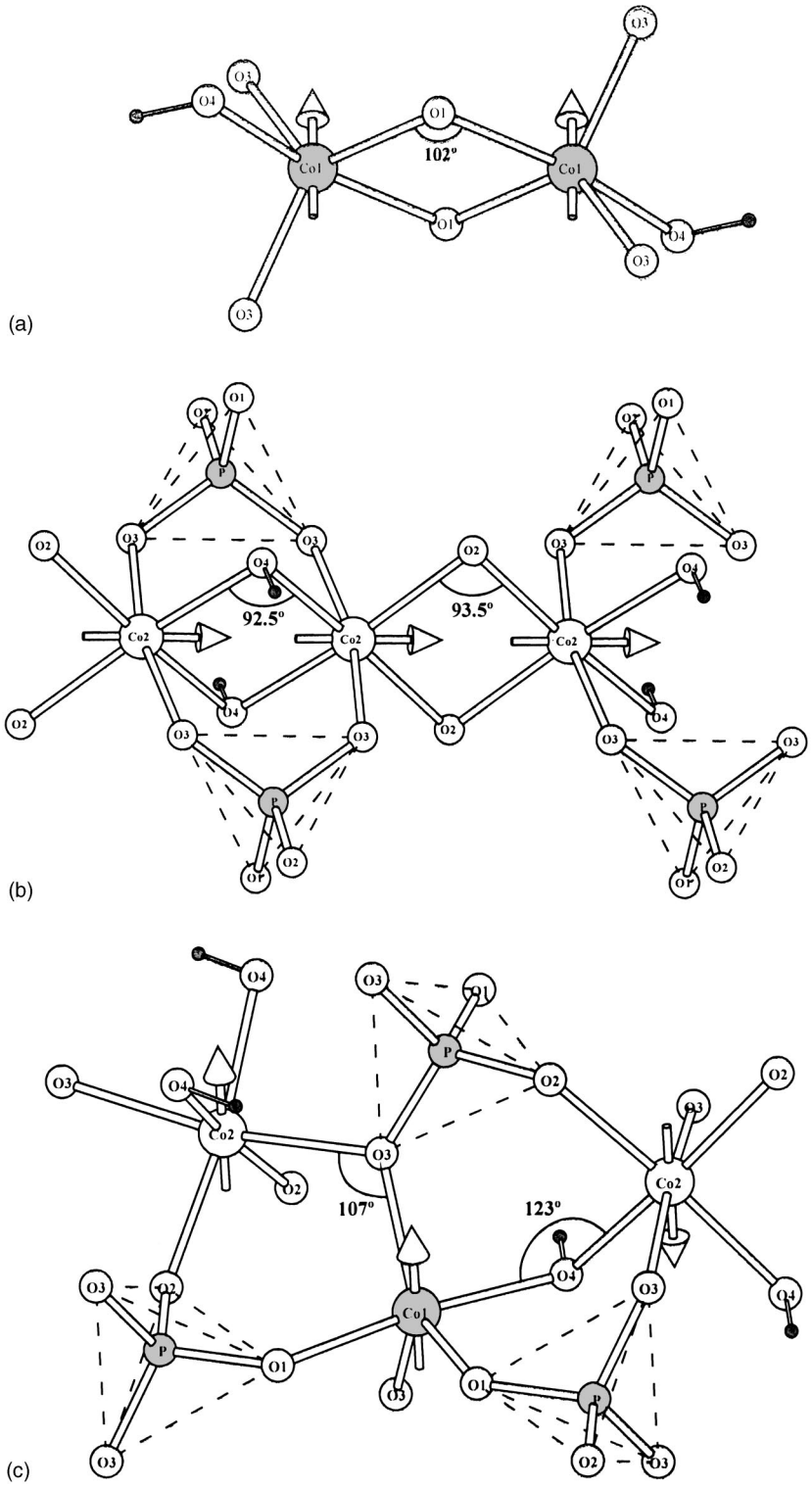

FIG. 14. Exchange pathways for $Co_2(OH)(PO_4)$. Interactions via (a) and (b) oxygen bridges of edge-sharing, (b) and (c) vertex oxygen bridges, and phosphate groups.

$B = 815\ cm^{-1}$ and $Dq = 905\ cm^{-1}$, the following values are obtained: $a = 0.9811$, $b = -0.1933$, $\alpha = -1.4063$, $\Delta' = 7953\ cm^{-1}$, and $k_o = 0.86$.

The magnetic study indicates the presence of an overall three-dimensional antiferromagnetic order between Co^{2+} ions at around 70 K. The signal observed at about 15 K in the low field magnetization measurements together with the existence of a ferromagnetic component confirm the presence of an anomaly, which looks to a spin-glass behavior, at this temperature in the cobalt hydroxyphosphate. The thermal dependence of the magnetic susceptibility of $Co_2(OH)(PO_4)$ shows a magnetic hysteresis between the ZFC and FC parts. The FC and ZFC magnetization curves start to separate at around 13 K, where a weak irreversibility begins to develop and magnetic correlation between magnetic moments appears. The difference between the FC and ZFC curves is

explained by the blocking of the magnetic moments in a paramagnetic state during the ZFC mode. Conversely, these moments are aligned parallel to the applied field during the FC mode; this leads to a larger magnetization in that case.[28] It is worth mentioning that the remanent magnetization $T = 7$ K changes its tendency, with an increase of $\approx 5\%$ by increasing the temperature up to $T \approx 13$ K [see Fig. 5(a)], this temperature being the same as that corresponding to the maxima in the ZFC-FC magnetization measurements. Magnetization under zero-field-cooled conditions falls below under field-cooled conditions at temperatures below T_f, a behavior observed in typical spin-glass materials. Although the canonical behavior associated with spin glasses, a constant FC magnetization while the ZFC magnetization drops toward zero, is only observed below 7 K, the appearance of irreversibility just below the maximum in the low-field magnetization curve together with the shape of the ZFC and FC curves confirm the spin-glass state suggesting a cooperative freezing at 13 K. A careful analysis of the FC branch clearly reveals the existence of a sudden increase of the magnetization below 22 K related, as we will see later, to the onset of the freezing process of the surface spin glass. Moreover, the strong irreversibility associated with the blocking process on the magnetic ions ($H < 1$ T) almost disappears for applied fields of 1 T (inset of Fig. 6) as it is expected when the anisotropy field of the ions is surpassed and magnetic moments are supposed to be saturated.

The presence of a spin-glass transition is also observed in the ac measurements from the data obtained at different frequencies and applied fields. The initial susceptibility at the lowest frequency measured (10 Hz) shows a cusp (Fig. 7) which has been considered as the spin-glass freezing temperature ($T_f \approx 13$ K). The maximum irreversibility decreases in both (χ') and (χ'') when the field increases and tends to disappear at about $H_{dc} \approx 2000$ Oe [see Fig. 7(c)]. This corresponds to the fact that the magnetic energy becomes sufficient (in a high field) to overcome the energy barrier (or blocking temperature) between the possible equilibrium positions of the magnetic moments. Moreover, the temperature of the maximum of the ZFC curve increases with increasing fields, which is reminiscent of the behavior of spin glasses. Furthermore, the magnetization shows a hysteresis loop with a nonzero remanent magnetization below T_f. These facts can be considered as a clear evidence for the formation of a spin-glass state in $Co_2(OH)(PO_4)$ with a freezing temperature at $T_f \approx 13$ K. All these results obtained from the magnetic measurements together with the no observation of a magnetic peak in the heat-capacity data at 13 K, whereas a broad anomaly in the magnetic specific heat appears well above this temperature (see Fig. 8) are a distinct feature of a spin glass state with a static freezing temperature that it is slightly dependent of the frequency,[29,30] and clearly indicates that usual long-range spatial magnetic order does not occur at T_f, so it is a system with a spin-glass phase of nearly 15 K.

The magnetic behavior of $Co_2(OH)(PO_4)$ shows the presence of two types of magnetic interactions: (i) three-dimensional antiferromagnetic interactions which dominate at high temperatures and that are the responsible for the high extrapolated negative Curie-Weiss temperature, and (ii) ferromagnetic interactions at temperatures lower than 20 K where the field-cooled magnetization (or susceptibility) increases. This fact can be explained as due to the existence of ferromagnetic domains into an overall antiferromagnetic behavior which predominates at high temperatures. The uncompensated moments caused by exchange interactions between the moments can be frozen below a blocking temperature which their relaxation time (τ_m) corresponds to the measuring time ($t = 1/\nu$) in ac susceptibility measurements. Although there is a distribution of blocking temperatures, the irreversibility appears below a peak, at T_f, in the ZFC magnetization measured in a low field or in the ac susceptibility. Depending on the interactions between the magnetic moments, T_f can be strongly (weak interactions) or weakly (strong interactions) dependent on the measuring time. In $Co_2(OH)(PO_4)$ the frequency shifts of the maxima in the χ' susceptibility, within the experimental errors, yield ratio $\Delta T_f / [T_f \Delta(\ln \nu)]$ of 0.0024 which is in good agreement with values previously reported for spin glasses.[29,31] The temperature dependence of τ_m may be described by the Vogel-Fulcher law with a relaxation time characteristic of strong interactions and weak frequency dependence of T_f:

$$\tau_m = \tau_o \exp\left[\frac{E_a}{k_B(T_f - T_o)}\right]. \tag{2}$$

As found experimentally for other spin glasses,[32] τ_m diverges at a temperature T_o which is smaller than the freezing temperature T_f. Assuming the variation of the χ' to a Gaussian function around the T_f and taking $\nu_o = \tau_o^{-1} = 10^{13}$ Hz,[32] we obtain reasonable fitting parameters $T_o = 13.6$ K and $E_a/k_B = 20.4$ K as compared to other data.[31] Therefore, the frequency dependence of the T_f is well described by the Vogel-Fulcher law [see the inset in Fig. 7(b)] as correspond to a spin-glass transition.

The magnetic structure of $Co_2(OH)(PO_4)$ (Fig. 10) consists of ferromagnetic arrangements between the Co(2) octahedral chains and Co(1) trigonal bipyramidal dimers within *xz* plane with the magnetic moments along the *z* direction. The magnetic interactions in each sublattice, $[Co(2)O_8]_\infty$ octahedral chains and $[Co(1)_2O_8]$ dimeric units, together with the interactions through the $|OH|$ and phosphate groups give rise to a three-dimensional antiferromagnetic coupling. The explanation for the observation of markedly different saturated magnetic moments in $Co_2(OH)(PO_4)$ with two chemically similar Co^{2+} cations must be based on the differences between the geometries around the two cation sites. Spontaneous static ordering of the magnetic moments at low temperatures is caused by exchange interactions between the moments, making it energetically favorable for them to align either parallel or anti-parallel. Superexchange interactions are well understood for a simple cation-anion-cation pathway with interactions strongly antiferromagnetic for a linear 180° Co-O-Co bond angle and ferromagnetic for an angle of 90° with the crossover at around 100.6°. The higher value observed up to now for ferromagnetic interactions in Co(II) compounds with Co-N bonds is 102.3°.[33]

The magnetic structure of $Co_2(OH)(PO_4)$ shows several exchange pathways[34–36] (see Fig. 14): (i) direct antiferromagnetic intradimeric interactions involving d_{yz} Co^{2+} orbitals from the Co(1) and Co(2) sublattices. (ii) Superexchange intradimer interactions via oxygen involving metal $d_{x^2-y^2}$ orbitals from edge-sharing both $[Co(1)_2O_8]$ trigonal bipyramidal dimers and $[Co(2)O_8]_\infty$ octahedra chains [see Figs. 14(a) and 14(b)]. These exchange pathways follow the *z* direction where the *c* parameter increases with decreasing temperature. The $Co(1)_2O_8$ and $[Co(2)O_8]_\infty$ ''sequences'' with angles of 92.5–93.5 and 102° respectively, favor ferromagnetic couplings. (iii) Superexchange interactions through the $|OH|$ groups, Co(1)-O(4)H-Co(2), between dimers and chains. The exchange pathways follow the *y* direction where the *b* parameter is practically constant in all temperature range studied. The interactions concerning this direction are clearly antiferromagnetic with an exchange angle of 123° [see Fig. 14(c)]. (iv) Ferromagnetic superexchange interactions between dimers and their neighbor chains, through the O(3) atoms, which are also ferromagnetically coupled [see Fig. 14(c)]. The ferromagnetic interactions observed in the *xz* plane, where the *a* parameter undergoes an unexpected behavior, are principally produced by the superexchange angle, Co(1)-O(3)-Co(2), that simultaneously involves, by symmetry, two exchange pathways with a value of 107°. This striking exchange angle, as far as we are aware, is the higher angle found in the literature for a ferromagnetic exchange pathway. Finally, (v) superexchange antiferromagnetic pathways through the $|PO_4|$ groups in $|CoO_5|$-$|PO_4|$-$|CoO_5|$ and $|CoO_5|$-$|PO_4|$-$|CoO_6|$ sequence [see Figs. 14(b) and 14(c)]. The $|OH|$ groups and the $|PO_4|$ tetrahedra allow to propagate the magnetic interactions giving rise to an antiferromagnetic three-dimensional system.

The thermal variation of the magnetic moments indicates that a rapid ordering between 70 and 50 K is established [see Fig. 13]. At 50 K the Co(2) magnetic moments in the chains reach approximately 90% of ordering, whereas the Co(1) ions in the dimers only reach 75%. Below 20 K, the magnetic moments of both sublattices are practically saturated with a difference between the ordered magnetic moments of approximately 10%. This difference could be attributed to the presence of two different causes (a) the distinct crystal field effects in both sublattices or (b) the existence of a spin glass state. Notwithstanding, both effects can act simultaneously. If we only consider the crystal electrical field, the Co(II) ions in each sublattice have ''real'' different magnetic moment as shown in Fig. 13, and in this case, we can describe our magnetic structure, strictly speaking, as ''antiferrimagnetic'' because each sublattice orders itself antiferromagnetically. However, if the differences in the magnetic moment are associated to the spin glass transition, only a fraction of the Co(1) moments periodically orders below the Neel temperature and a certain percentage remains disordered until the spin glass transition is reached becoming randomly freeze. In this framework, the values of the magnetic moment extracted from the fitting to the diffraction patterns are ''effective'' magnetic moments in the ordered state. This means that the Co(1) and Co(2) magnetic moments have the same value. The differences given in Fig. 13 can be explained by considering that all the magnetic moments in the sublattice *S* participate of the long range antiferromagnetic order. However, in the sublattice *R*, only 90% of Co(1) moments became ordered and the rest is contributing to the freezing processes. Because neither Co(1) nor Co(2) magnetic moments reach the full free-ion moment expected for Co(II) we can consider that both effects are present: the crystal field reducing the moment in both sublattices and the random freezing of Co(1) moments decreasing the ''effective'' magnetic moment of the sublattice *R*. Another interesting point to be considered with respect to the freezing processes is the existence of magnetic frustration in the Co(1) present in the dimers due to the existence of antiferromagnetic interactions between the Co(2) neighbor chains [see Fig. 14(c)].

On the other hand, it is worth mentioning the effect of the Co(1)-O(3)-Co(2) angle in the magnetic behavior of $Co_2(OH)(PO_4)$. The value of this angle, 107°, does not undergo any variation with the temperature from room temperature to 2 K. This angle can be considered as an orthogonal ''accidental'' angle giving rise to the different disposition of the moments which is essential to install the competition and ensure cooperativeness of the freezing process. The decrease in temperature below 20 K shows that these moments can be regarded as a spin glass state. Preliminary results in the arsenate $Co_2(OH)(AsO_4)$ phase indicate a variation of this angle from 114.5° at 300 K and 113° at 100 K. Below 20 K the magnetic structure is completely different and an incommensurate phase is observed. Considering all these data we finally propose that the anisotropy of Co^{2+} ions, the frustration of the Co(1) magnetic moments and the Co(1)-O(3)-Co(2) angle play an important role in the presence of a spin-glass behavior in the $Co_2(OH)(PO_4)$ ordered phase.

V. SUMMARY

Two anomalies of magnetic origin can be observed at 70 and 13 K in $Co_2(OH)PO_4$ by different magnetic techniques (dc and ac) as well as in thermal evolution of the cell parameter. The anomaly at higher temperature is clearly due to the establishment of long-range antiferromagnetic order. The absence of any distinguishing anomaly in the heat capacity at 13 K as well as the fact that the magnetic structure does not change between 70 and 2 K, strongly support previous evidence in the magnetic measurements about the spin-glass nature of the low-temperature transition. Therefore, we can conclude than in $Co_2(OH)PO_4$ a spin-glass freezing coexists, with the long-range-antiferromagnetic order below 13 K comprising the freezer moments, which correspond to Co(1) ions along the *z* direction.

ACKNOWLEDGMENTS

This work was financially supported by the Ministerio de Educación y Ciencia (PB97-0640; BQU2001-0678) and the Universidad del País Vasco/EHU (9/UPV00169.310-13494/2001; 9/UPV00130.310-13700/2001), which we gratefully acknowledge. We thank M. T. Fernández-Díaz from the Institute Laue-Langevin (ILL) Grenoble, France for help in the neutron diffraction measurements carried out in the D1B and D2B powder diffractometers.

*Present address: Departamento de Química Inorgánica, Facultad de Ciencias, Universidad del País Vasco, Apdo. 644, E-48080 Bilbao, Spain. Email address: qiproapt@lg.ehu.es FAX: 34-944648500

[1] R. C. Haushalter and L. A. Mundi, Chem. Mater. **4**, 31 (1992).
[2] A. Clearfield, Chem. Rev. **88**, 125 (1988).
[3] W. E. Richmond, Am. Mineral. **25**, 441 (1940).
[4] F. C. Hawthorne, Can. Mineral. **14**, 143 (1976).
[5] P. B. Moore and J. R. Smythe, Am. Mineral. **53**, 1841 (1968).
[6] A. Cordsen, Can. Mineral. **16**, 153 (1978).
[7] H. Heritsch, Z. Kristallogr. **99**, 466 (1938).
[8] C. B. Burnham and M. J. Buerger, Z. Kristallogr. **115**, 269 (1961).
[9] P. Keller, Neues Jahrb. Mineral. Monatsh. **1971**, 560.
[10] W. T. A. Harrison, J. T. Vaughey, L. L. Dussack, A. J. Jacobson, T. E. Martin, and G. D. Stucky, J. Solid State Chem. **114**, 151 (1995).
[11] T. Rojo, L. Lezama, J. M. Rojo, M. Insausti, M. I. Arriortua, and G. Villeneuve, Eur. J. Solid State Inorg. Chem. **29**, 217 (1992).
[12] H. M. Rietveld, J. Appl. Crystallogr. **2**, 65 (1969).
[13] J. Rodríguez-Carvajal, *FULLPROF Program for Rietveld Refinement and Pattern Matching Analysis of Powder Patterns*, 1998 (unpublished). The program is a strongly modified version of that described by D. B. Wiles and R. A. Young, J. Appl. Crystallogr. **14**, 149 (1981).
[14] A. B. P. Lever, *Inorganic Electronic Spectroscopy* (Elsevier, London, 1984).
[15] R. L. Carlin, *Magnetochemistry* (Springer, Berlin, 1986).
[16] A. Abragam and M. H. L. Pryce, Proc. R. Soc. London, Ser. A **200**, 173 (1951).
[17] J. M. Rojo, J. L. Mesa, L. Lezama, G. E. Barberis, and T. Rojo, J. Magn. Magn. Mater. **157/158**, 493 (1996).
[18] G. Villeneuve, J. L. Pizarro, J. M. Dance, M. I. Arriortua, T. Rojo, and R. Kuentzler, J. Magn. Magn. Mater. **83**, 478 (1990).
[19] J. J. Borras-Almenar, E. Coronado, D. Gatteschi, and C. Zanchini, Inorg. Chem. **31**, 294 (1992).
[20] J. M. Rojo, J. L. Mesa, J. L. Pizarro, L. Lezama, M. I. Arriortua, and T. Rojo, J. Solid State Chem. **132**, 107 (1997).
[21] M. E. Foglio, M. C. dos Santos, G. E. Barberis, J. M. Rojo, J. L. Mesa, L. Lezama, and T. Rojo, J. Phys.: Condens. Matter **14**, 2025 (2002).
[22] C. S. Lue, Y. Oner, D. G. Naugle, and J. H. Ross, Phys. Rev. B **63**, 184405 (2001), and references therein.
[23] E. F. Bertaut, Acta Crystallogr., Sect. A: Cryst. Phys., Diffr., Theor. Gen. Crystallogr. **24**, 217 (1968).
[24] A. Abragam and B. Bleaney, *Electron Paramagnetic Resonance of Transition Ions* (Clarendon, Oxford, 1970), Sec. 7.14, p. 447.
[25] M. Tinckham, Proc. R. Soc. London, Ser. A **236**, 549 (1956).
[26] L. T. Peixoto and M. E. Foglio, Rev. Bras. Fis. **13**, 564 (1983).
[27] E. B. Tucker, Phys. Rev. **143**, 264 (1966).
[28] H. Mamiya, I. Nakatani, and T. Furubayashi, Phys. Rev. Lett. **80**, 177 (1998).
[29] K. Moorjani and J. M. D. Coey, in *Magnetic Glasses*, edited by S. P. Wolsky and A. W. Czanderna, Methods and Phenomena Vol. 6 (Elsevier, Amsterdam, 1984). K. H. Fischer and J. Hertz, *Spin Glasses* (Cambridge University Press, Cambridge, England, 1991).
[30] J. M. De Teresa, M. R. Ibarra, J. García, J. Belasco, C. Ritter, P. A. Algarabel, C. Marquina, and A. Del Moral, Phys. Rev. Lett. **76**, 3392 (1996).
[31] J. A. Mydosh, *Spin Glasses: An Experimental Introduction* (Taylor & Francis, London, 1993).
[32] J. L. Tholence, Solid State Commun. **35**, 113 (1980).
[33] M. G. Barandika, Z. Serna, R. Cortes, L. Lezama, M. K. Urtiaga, M. I. Arriortua, and T. Rojo, Chem. Commun. **2001**, 45; Z. Serna, M. K. Urtiaga, M. G. Barandika, R. Cortes, L. Lezama, M. I. Arriortua, and T. Rojo, Inorg. Chem. **40**, 4550 (2001).
[34] J. B. Goodenough, *Magnetism and the Chemical Bond* (Interscience, New York, 1963).
[35] O. Khan, Inorg. Chem. **3**, 105 (1984).
[36] O. Khan, Struct. Bonding (Berlin) **68**, 89 (1987).